Sensors & Transducers, Vol. 226, Issue 10, October 2018, pp. 1-9

www.sensorsportal.com

Sensors & Transducers

Published by IFSA Publishing, S. L., 2018
http://www.sensorsportal.com

Applications of Modern Controls for Laser Jitter and Wavefront Correction

[1] Jae Jun Kim and [2] Brij Agrawal
Naval Postgraduate School, 1 University Circle, Monterey, CA 93943
[1] Tel.: +1-831-656-2716, fax: +1-831-656-3111
[1] E-mail: jki1@nps.edu

Received: 25 June 2018 /Accepted: 31 August 2018 /Published: 31 October 2018

Abstract: Optical beams are used in many applications, such as imaging, laser communications, and high energy laser systems. Performance requirements of optical beams for acquisition, tracking, pointing, jitter control, and wave front correction control are very challenging. Advanced optics and controls techniques have been developed to meet these requirements. This paper provides an application of modern control methods such as adaptive filter control and modal control, aiming to increase the performance of optical jitter and wavefront aberration compensation. Experimental results are also presented to demonstrate the effectiveness of these control methods.

Keywords: Wavefront sensor, Adaptive optics, Optical beam, Jitter, Wavefront aberration, Adaptive filter, Modal control.

1. Introduction

Optical beams are used in many applications, such as imaging, laser communications, and high energy laser systems. Performance requirements of optical beams for acquisition, tracking, pointing, jitter control and wave front correction control are very challenging.

As an example of the Hubble Space Telescope, the beam pointing requirement is 0.012 arc sec (0.000003 degree) jitter, pointing stability, requirement is 0.007 arc-secs (0.000002 degree). Several passive and active techniques have been developed to reduce optical beam jitter [1-2]. In general, passive techniques systems perform best for higher frequencies, typically greater than 5 Hz, while active systems perform best for lower frequencies, typically lower than 5 Hz. Most spacecraft jitter control solutions require a hybrid system (passive and active) to suppress the entire range of disturbance frequencies. This paper will provide experimental results of active jitter control using modern control techniques.

Wavefront aberration in an optical beam can be caused by many sources, such as imperfection in optical components and atmospheric turbulence. Wavefront aberration adversely impacts the performance of imaging system in terms of resolution, in laser communications in terms of bit error rates, and in high energy lasers in terms of intensity of the beam. Adaptive optics has been used to correct the wavefront aberration in optical beams. A typical adaptive optics system for ground telescope is shown in the Fig. 1.

Adaptive optics system consists of a reference beam that passes through the same path as the target object beam and the wavefront error is measured by a wavefront sensor, such as Shack Hartman sensor. Using the wavefront error information from the sensor and using control feedback laws, surface of a deformable mirror is distorted to compensate for wavefront error. When the object beam now passes through the deformable mirror, the wavefront is corrected. Deformable mirrors have hundreds of actuators, such as piezoceramic actuators on the back to deform the mirror surface to compensate for

wavefront error. The output of the wavefront error is measured in hundreds; therefore the feedback control is complex thus becoming multi-input and multi-output.

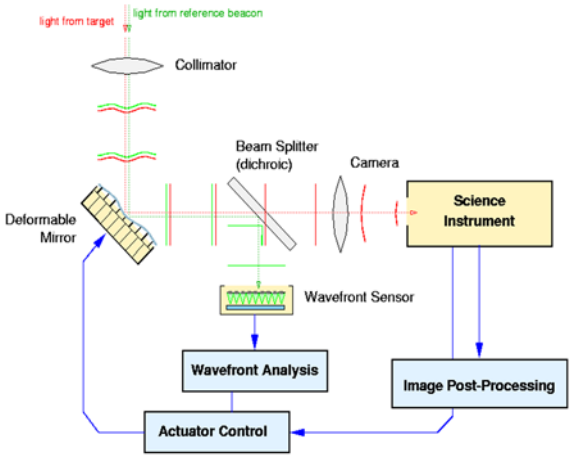


Fig. 1. Wavefront Aberration Compensation Using Adaptive Optics (from [3]).

The classical control algorithm for adaptive optics ignores the dynamics of the system plant including deformable mirror and wave front sensors. The static relationship between control input from deformable mirror and wavefront sensor output is written as

$$\mathbf{y} = \Phi\mathbf{u}, \tag{1}$$

where y is the sensor output, Φ is called the poke matrix or influence matrix obtained by actuating one sensor at a time and u is actuator input. Simple integral control algorithm typically used is

$$\mathbf{u}(k) = \mathbf{u}(k-1) + \mu\Phi^{\dagger}\mathbf{y}(k), \tag{2}$$

where $\Phi^{\dagger}$ is the pseudo inverse of Φ.

In actual system, dynamics cannot be ignored and the atmospheric turbulence is also fast changing at the rate of several kHz. Therefore high spatial and temporal frequency correction is needed for such systems. For wavefront aberration correction using adaptive optics, performance can be significantly improved by using modern control techniques such as adaptive filters and modal control. This paper will provide these control methods applied to the adaptive optics problem for wavefront aberration correction. Experimental wavefront correction results are also presented using adaptive filter control techniques.

2. Adaptive Filter

The basic principle of an adaptive filter is that controller gains can be varied throughout the control process to adapt to changing parameters and can therefore cancel disturbances more effectively than with fixed gains. Transverse Finite Impulse Response (FIR) filter structure was used for the adaptive filter control method. Least Mean square (LMS) and Recursive Least Square (RLS) algorithms were used to update the weights in the transverse filter.

An L^{th} order transverse FIR filter has the structure shown in Fig. 2. Each of the L stages, or taps, delays the input signal by one sample, which leads many to call this filter a tapped-delay line. The filter output is expressed as follows:

$$y(n) = \sum_{i=0}^{L} w_i(n)x(n-i) = \mathbf{w}^{\mathrm{T}}(n)\mathbf{x}(n), \tag{3}$$

where $\mathbf{w}(n)$ is the filter weight vector of length L whose i^{th} component is $w_i(n)$, $\mathbf{x}(n)$ is the vector of delayed inputs, $x(n-i)$ and $y(n)$ is the filter output.

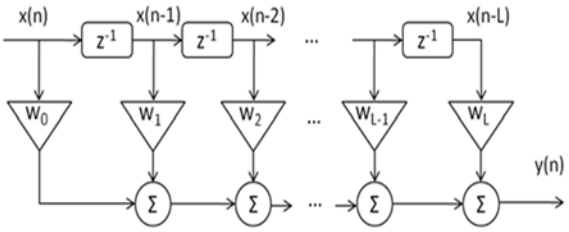


Fig. 2. Transverse FIR filter structure.

Fig. 3 shows the simplest implementation of a feedforward adaptive algorithm. The function of the adaptive filter is to modify an incoming or reference signal, $x(n)$, to cancel a disturbance applied to the system. Using a transverse filter and a reference that is correlated with the disturbance, the filter delays the incoming signal $L-1$ times and multiplies the resulting vector by a set of L weights, as shown in Fig. 3. The error, $e(n)$, is measured at an error sensor and is the difference between the applied disturbance and the filter output, $y(n)$, which is the canceling signal from the adaptive filter.

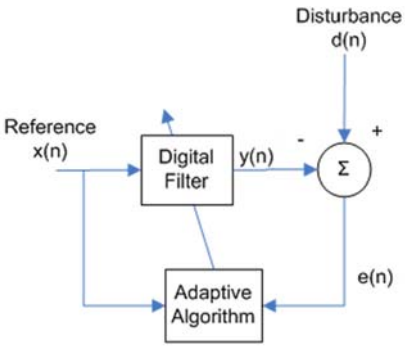


Fig. 3. Simple implementation of adaptive algorithm.

The adaptive weights are computed by an algorithm that uses the reference and error signals to minimize a cost function. In the LMS algorithm, the

cost function is the mean square error (MSE), which is the expectation of $e(n)^2$ and is denoted by $\zeta(n)$.

When the statistics of the disturbance and the reference signal are available, the weights that minimize the MSE can be computed. In practice, however, such a priori information is often unavailable. As a result, the MSE is approximated by the instantaneous squared error and minimized using iterative steepest-gradient descent to update the weights in the direction of lowest error. The resulting form of the LMS algorithm is expressed as:

$$\mathbf{w}(n+1) = \mathbf{w}(n) + \alpha \mathbf{x}(n) e(n), \qquad (4)$$

where α is the convergence coefficient that controls the speed at which the algorithm converges to steady-state weight values.

In reality, the basic adaptive algorithm must be modified because the control signal passes through a physical actuator before its effect is sensed at the error sensor. A secondary path or plant transfer function, $S(z)$, contains information on the interaction between sensor and actuator and is denoted by the S block in the augmented diagram in Fig. 4. Its effect on the control action must be taken into account to prevent instability and ensure that the filter,W, cancels the disturbance after the secondary plant, and not before.

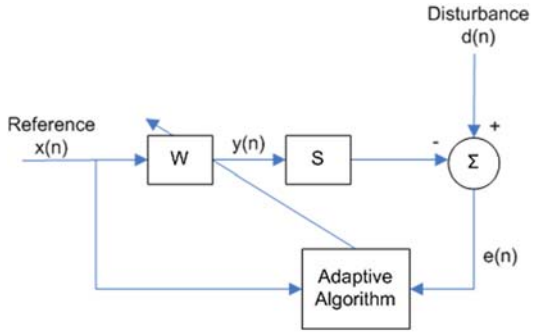


Fig. 4. Adaptive algorithm showing secondary plant after filter output.

To account for the secondary plant dynamics, the reference signal is passed through a copy or estimate of the secondary plant, $\hat{S}(z)$, before being used in the adaptive algorithm. The LMS algorithm is updated as:

$$\mathbf{w}(n+1) = \mathbf{w}(n) + \alpha \mathbf{r}(n) e(n), \qquad (5)$$

where $\mathbf{r}(n)$ represents the filtered reference, $\mathbf{r}(n) = \hat{s}(n) * \mathbf{x}(n)$. As such, this method is called Filtered-x LMS, or FXLMS. The complete FXLMS model is shown in Fig. 5.

The practical challenge with the adaptive filters described so far is that they require a reference signal that is correlated with the disturbance in order to provide feedforward correction and canceling. In lieu of an external reference, it is possible to generate an internal reference that is an estimate of the disturbance [1]. This reference is produced by passing the adaptive filter output through another estimate of the secondary plant and adding this output to the error signal. This effectively removes the adaptive filter output from the error, leaving only an estimate of the disturbance. If the secondary plant model is precise, the reference signal becomes the disturbance itself. The reference signal is expressed as:

$$x(n) = e(n) + \hat{s}(n) * y(n) = \hat{d}(n), \qquad (6)$$

with "$*$" denoting the convolution operation. Fig. 6 shows the modified controller diagram in which the reference signal is generated.

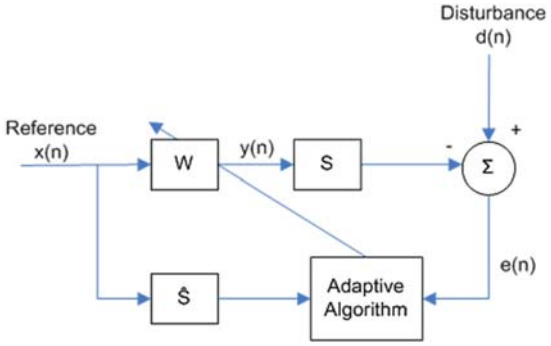


Fig. 5. FXLMS structure including secondary plant estimate prior to adaptation.

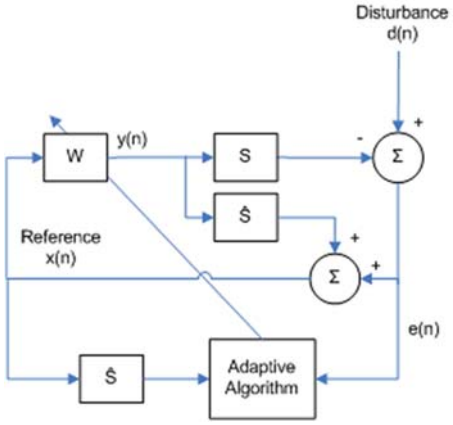


Fig. 6. Adaptive controller diagram with internally generated reference.

The need to estimate the disturbance from the error adds a delay in the system and turns a previously feedforward controller into a feedback controller. As such, the ability of a true feedforward controller to address broadband disturbances becomes limited.

Adaptive filter with classical control loop

The classical controller considered for this paper is a Proportional-Integral (PI) controller, denoted by $C(z)$ in discrete form and expressed as

$$C(z) = \frac{K_i z}{z-1} + K_p, \qquad (7)$$

where the integral gain, K_i, and the proportional gain, K_p, are designed to meet reasonable specifications of the PI control loop, and the discrete sample time, T_s, is included in the integral gain. The adaptive filter is expected to improve the overall controller performance for disturbances which are outside the bandwidth of the PI controller.

The combination of the adaptive controller with internally generated reference and the PI controller is shown in Fig. 7. The system delay, z^{-q}, is included and can represent a delay of any number of time steps, q.

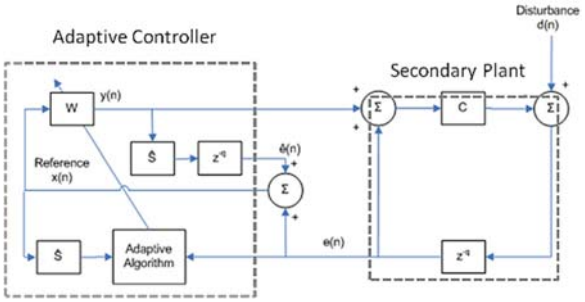


Fig. 7. Final configuration of adaptive and PI controllers together.

Multichannel LMS/FXLMS Adaptive Filter

For jitter control, single input and single output is adequate. However, an adaptive optics system is a Multiple Input Multiple Output (MIMO) system, the LMS and FXLMS adaptive algorithms must be extended for use with multiple channels. Multiple error LMS was proposed by Elliott, *et al.* [4], for multichannel active noise control applications. The summation notation here draws from Elliott, while for consistency most of the variables again follow Kuo [1]. In a multichannel adaptive filter algorithm, the number of reference signals can be independent of the number of sensors or actuators. For M error sensors, K control actuators, and J reference signals, there are $M \times K$ secondary path models and $K \times J$ weight vectors. Each of the weight vectors is length L, so that the actual size of the weight matrix or filter W is $K \times JL$. Each secondary path model, s_{mk} represents the relationship between the control action by the k^{th} actuator and the error observed by the m^{th} sensor. For the rigid deformable mirror whose dynamics are ignored, the mirror's contribution to the secondary path model consists of the elements of the poke matrix, each of which represents the interaction between a particular mirror actuator and Shack-Hartmann wavefront sensor lenslet. The command for the k^{th} actuator is generated by multiplying each of the J reference signals by its corresponding weight vector and is expressed as

$$y_k(n) = \sum_{j=1}^{J} \mathbf{w}_{kj}^T(n)\mathbf{x}_j(n), \tag{8}$$

where $\mathbf{w}_{kj}(n) = \left[w_{kj0}(n) \cdots w_{kj(L-1)}(n)\right]^T$, the complete command vector is given by $\mathbf{y}(n) = [y_1(n)\, y_2(n) \cdots y_k(n)]^T$, and the complete reference vector is given by $\mathbf{x}(n) = \left[x_1^T(n)\, x_2^T(n) \cdots x_j^T(n)\right]^T$. The weight update equation is simply the multichannel expression of the FXLMS algorithm shown before and is given by:

$$\mathbf{w}_{kj}(n+1) = \mathbf{w}_{kj}(n) + \alpha \sum_{m=1}^{M} \mathbf{r}_{kjm}(n)\mathbf{e}_m(n), \tag{9}$$

where $\mathbf{e}(n) = [e_1(n)\, e_2(n) \cdots e_M(n)]^T$, and the filtered reference is $\mathbf{r}_{kjm}(n) = s_{mk}(n) * \mathbf{x}_j(n)$.

RLS Adaptive Filter

The Recursive Least Squares algorithm follows much of the development shown for LMS, with the important exception that it includes past data in its cost function. This accommodates nonstationary signals and usually provides faster convergence and smaller steady-state error than the LMS algorithm, though it is more computationally complex [1]. Instead of expressing the MSE as the instantaneous squared error signal only, the cost function becomes

$$\zeta(n) = \sum_{i=1}^{n} \lambda^{n-i} e^2(i), \tag{10}$$

where the forgetting factor, $0 < \lambda \leq 1$, allows more recent data to be weighted more heavily and data long past to be forgotten. A value of $\lambda = 1$ implies that nothing is forgotten, while smaller values allow more forgetting. As it is desirable to use as much information as possible, values of λ used in the NPS jitter control testbeds range from 0.9–0.99999.

While the error and control signal expressions in RLS are identical to those of LMS, the weight update process is different. Optimal weights could be calculated from the statistics of the reference and disturbance signals if they are available, but such computation is extremely difficult for large sample times. Instead of calculating and inverting the correlation matrix of the reference input, $\mathbf{R}(n)$, the inverse correlation matrix, $\mathbf{Q}(n) = \mathbf{R}^{-1}(n)$ is calculated recursively. This eliminates the need to compute or invert $\mathbf{R}(n)$, greatly reducing the complexity of the RLS algorithm. The recursive equations for weight updates using the filtered reference for FXRLS formulation are:

$$\mathbf{z}(n) = \lambda^{-1}\mathbf{Q}(n-1)\mathbf{r}(n), \tag{11}$$

$$\mathbf{k}(n) = \frac{\mathbf{z}(n)}{\mathbf{r}^{\mathrm{T}}(n)\mathbf{z}(n) + 1}, \tag{12}$$

$$\mathbf{w}(n+1) = \mathbf{w}(n) + \mathbf{k}(n)e(n), \tag{13}$$

where $\mathbf{z}(n)$ is an intermediate calculation and $\mathbf{k}(n)$ is the current gain vector. Finally, the inverse sample correlation matrix is updated as:

$$\mathbf{Q}(n) = \lambda^{-1}\mathbf{Q}(n-1) - \mathbf{k}(n)\mathbf{z}^{\mathrm{T}}(n) \qquad (14)$$

Initial condition of $\mathbf{Q}$ is a diagonal matrix whose component is determined by the expected variance of the measurement noise.

$$\mathbf{Q}(0) = \frac{1}{\sigma_m^2}\mathbf{I} \qquad (15)$$

3. Modal Control

Adaptive optics control is a Multi-Input Multi-Output (MIMO) control problem, but it can be converted to a set of Single-Input Single-Output (SISO) through modal decomposition and SISO control schemes can be applied to each control channel. Fig. 8 shows a typical feedback control schematic of an adaptive optics system.

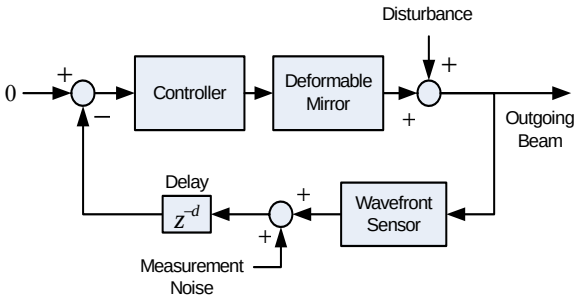


Fig. 8. Adaptive Optics Feedback Control System Diagram.

When a deformable mirror and a wavefront sensor is modelled as a poke matrix, Φ, equivalent control system diagram is shown in Fig. 9, where $\mathbf{y}$ is the output from a adaptive optics system plant, $\mathbf{d}$ is the disturbance, $\mathbf{v}$ is the sensor noise, $\mathbf{e}$ is the error, and $\mathbf{u}$ is the control input.

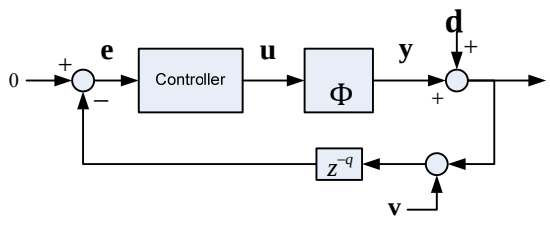


Fig. 9. Equivalent System Diagram.

The objective of designing a controller is to find a filter which produces the DM command signal from the observed error which keeps the feedback loop stable and provides desired performance for rejecting the effect of the disturbance in the output. In order to take advantage of using the design techniques developed for SISO system, one can introduce a so-called "reconstructor" in the control system.

Fig. 10 shows the system diagram when the reconstructor is added into the control system, where the new reconstructed error, $\mathbf{e}_c$, is used for the controller instead of the original error, $\mathbf{e}$.

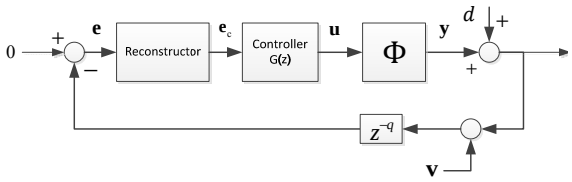


Fig. 10. Reconstructor in the Control System Diagram.

A simple form of recontructor is using the pseudo-inverse of the poke matrix, $\Phi^{\dagger}$. When $\Phi^{\dagger}$ is used as the reconstructor,

$$\mathbf{e}_c(k) = \Phi^{\dagger}\mathbf{e} = -\Phi^{\dagger}\mathbf{y} = -\Phi^{\dagger}\Phi\mathbf{u} = -\mathbf{I}\mathbf{u} \qquad (16)$$

assuming disturbance, noise, and time-delay is not present. Equation (16) represent the SISO relationship between the control channels and the control system error. Therefore, SISO control system design techniques can be applied.

One can further generalize the reconstructor concept and develop modal control approach using different modal basis.

Fig. 11 shows the block diagram of a modal control system where $\mathbf{F}$ represents the modal matrix where each colume represents differnt mode shape selected. Matrix $\mathbf{G}$ needs to be introduced in the control system to maintain the SISO properties, where

$$\mathbf{G} = (\mathbf{F}\Phi)^{\dagger} \qquad (17)$$

When $\Phi^{\dagger}$ is used as the reconstructor ($\mathbf{F} = \Phi^{\dagger}$) as shown previously, the matrix $\mathbf{G}$ becomes identity matrix. This modal control allows us to scale the dimension of the controller design space by selecting a proper modal basis. Modal reduction by retaining only significant modes through this modal control scheme can provide computationally efficient and robust control design. The matrix $\mathbf{F}$ projects the wavefront sensor information using a modal basis represented by the columns of the matrix $\mathbf{F}$. Therefore, one can have freedom to select an appropriate scalable modal basis to reconstruct the wavefront error information used by the controller.

Fig. 12 shows the visualization of example modal basis using a Shack-Hartmann wavefront sensor with 127 lenslet array [5]. Fig. 12(a) shows the poke matrix basis where the each mode is based on the influence function of a deformable mirror. Mode shape is determined based on Zernike polynomials in Fig. 12(b). Fig. 12(c) shows the modes based on singular value decomposition of a deformable mirror influence matrix (Poke matrix). Therefore, the mode

shapes are ordered by the effectiveness of the deformable mirror actuation.

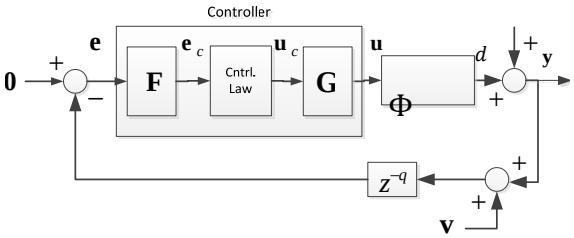
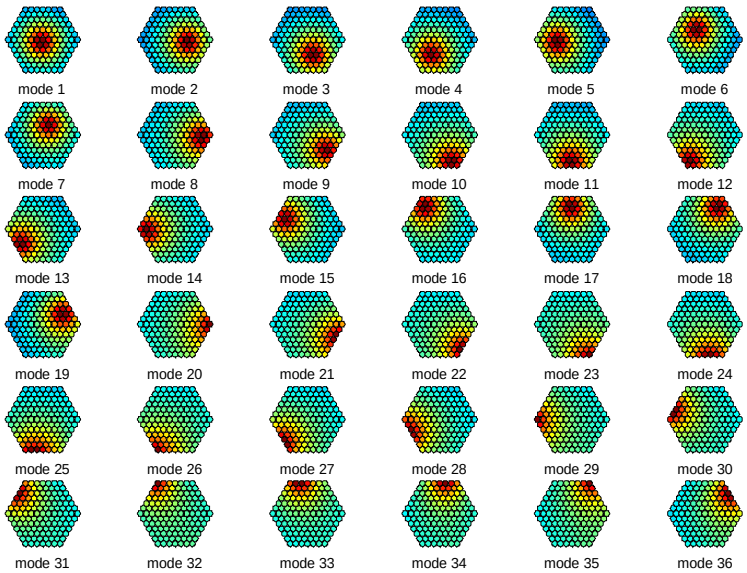
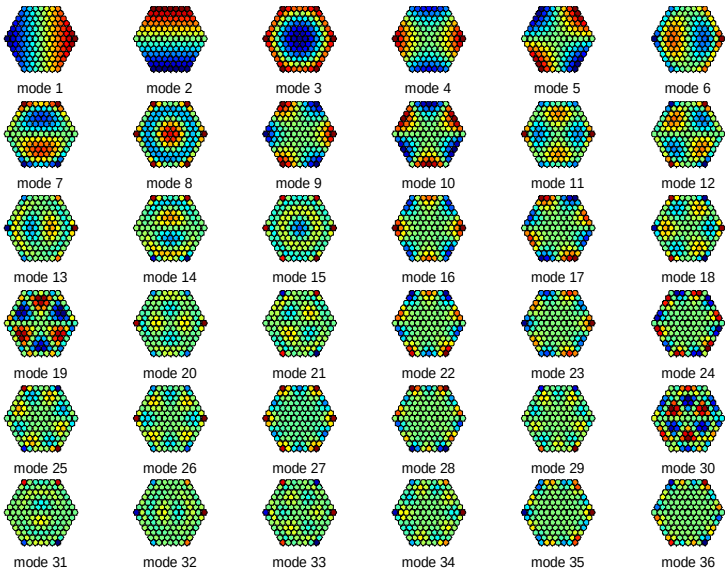


Fig. 11. Block Diagram of a Modal Control System.

In many cases, practical degree of freedom of a deformable mirror could be less than the required resolution of the correction. Therefore, trying to reconstruct the phase as accurately as possible is not necessary in order to achieve maximum performance with the given deformable mirror. With the modal decomposition technique, the controller can select the modes with the most contribution to the error reduction and ignore the modes with least contribution to save significant computation. In addition, ignoring the modes for which the deformable mirror is not effective or the measurement noise is high, can improve the robustness of the system. Applying a control law in modal coefficient space does not require explicit reconstruction of the phase, which may be beneficial for many practical adaptive optics control systems.

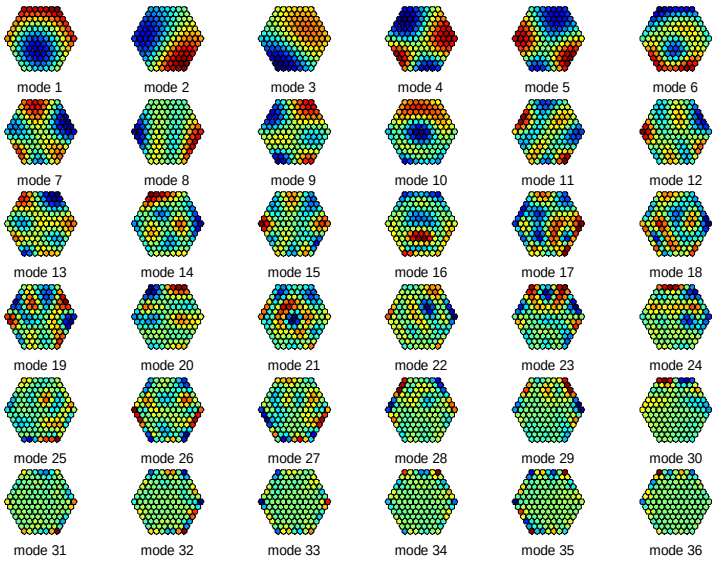


(a) Poke Matrix (Influence Matrix) Basis



(b) Zernike Polynomial Basis

Fig. 12 (a-b). Different Modal Basis Applied for Adaptive Optics Control.



(c) Singular Value Decomposition (SVD) Basis

Fig. 12 (c). Different Modal Basis Applied for Adaptive Optics Control.

4. Active Jitter Control Testbed

Jitter control is a pre-requisite for applying wavefront correction since the magnitude of the tip/tilt jitter is typically not corrected with a deformable mirror due to the limited actuator stroke. Jitter control can also benefit from the adaptive filter control discussed in Section 2. To demonstrate active techniques for optical beam jitter control, a Laser Jitter Control (LJC) testbed was developed at NPS. The components are mounted on a Newport optical bench, which can be floated to isolate the components from external vibrations. The laser beam originates from a source and passes through a Disturbance Injection Fast Steering Mirror (DFSM). The DFSM corrupts the beam using random or periodic disturbances simulating disturbances that might originate with the transmitting station or tip and tilt errors which the beam may suffer as it passes through the atmosphere. A control Fast Steering Mirror (FSM), designated the CFSM, is used to correct the disturbed beam. The corrected beam is then reflected off the platform to the target Position Sensing Detector (PSD). The schematic of the testbed is shown in Fig. 13.

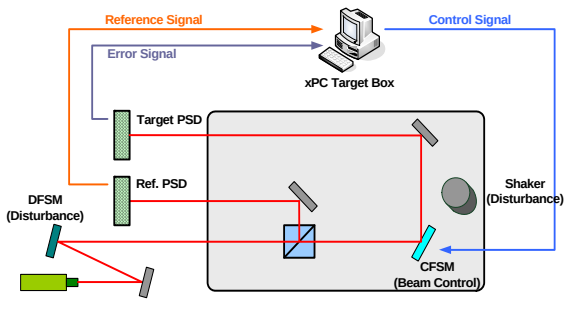


Fig. 13. Schematic of Laser Jitter Control Testbed.

Experimental results, shown in Fig. 14 demonstrated that the adaptive filters RLS provide significantly better performance.

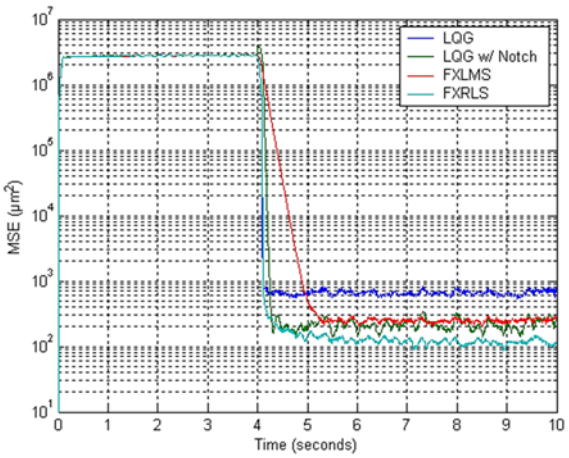


Fig. 14. Mean squared Error for Jitter Control Methods.

5. Experimental Testbed for Wavefront Correction

The adaptive filter technique discussed in Section 2 is also applicable for wavefront correction experiments [5-8]. Fig. 15 shows the adaptive optics testbed with primary components labeled.

Laser beam goes to two spatial light modulators, that add atmospheric aberration to the laser beam, next it goes to fast steering mirror that adds jitter to the laser beam, next it goes to deformable mirror for correcting aberration, next it is split up, one part goes to Shack Hartmann wavefront sensor, that measures wavefront aberration and is used to determine control input to the

actuators of the deformable mirror and the other part goes to science camera to measure laser quality, such as point spread function. The deformable mirror used in this testbed is an OKO 37-channel micromachined membrane deformable mirror (MMDM). The Shack-Hartmann (SH) wavefront sensor (WFS) is an OKO device with an array of 127 lenslets arranged in a hexagonal pattern. The array is attached directly to a Basler A601f camera with a resolution of 640×480 pixels and an 8-bit frame rate of approximately 20 fps. The liquid crystal (LC) spatial light modulator (SLM) used in the testbed is a Holoeye LC2002 device with 800×600 pixels of resolution and an operational rate of 33 Hz. The Naval Research Laboratory (NRL) has developed software to apply atmospheric aberrations on the SLMs using a Matlab graphical user interface (GUI). The atmosphere generated in software is based on traditional Kolmogorov statistics. The laser used is a continuous wave CVI Melles Griot Helium Neon Class II laser with output power of 0.5 mW, operating at a wavelength of 633 nm. The science camera is an IDS uEye-2210SE CCD camera with a resolution of 640×480 pixels and an 8-bit frame rate of 75 fps. It is used to capture images of the corrected and uncorrected beam.

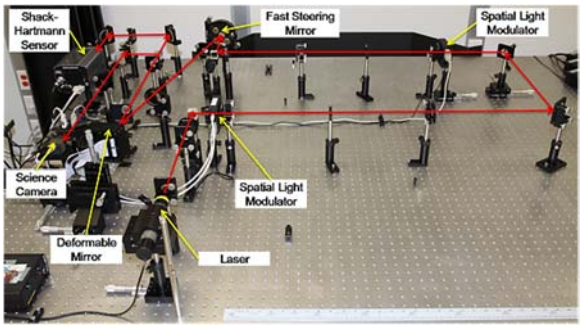


Fig. 15. Laboratory Testbed for Wavefront Correction.

Wavefront Correction Results Using Adaptive Filter Control

All testbed results presented are obtained from applying an atmospheric profile one SLM only. The atmospheric profile generated is for a telescope aperture of 1 m diameter and an atmospheric coherence length of $r_0 = 15$ cm, representing an atmosphere of medium strength. The atmosphere is run at 7.5 Hz on the SLMs, as the AO loop using a Simulink hardware interface can run currently at a maximum rate of 15 Hz. This rate is limited by the camera and can be improved with the introduction of a camera with a faster frame rate. In reality, the atmosphere changes more on the order of 100 Hz or higher. If desired, the testbed disturbance can be artificially sped up in simulation by decreasing the sample time of the controller.

Classical proportional and integral control (PI), LMS adaptive filter, and combined LMS adaptive filter and PI control laws are used. For PI control, K_i is 0.14 and K_p is 0.06.

Fig. 16 shows wavefront rms errors using PI, LMS adaptive filter, and combined PI and LMS adaptive filter. Table 1 shows the average RMS error in comparing the PI, LMS AF, and LMS AF + PI algorithms. As reflected in Fig. 16, the LMS AF works slightly better than the PI alone, while the combination of LMS AF + PI works the best overall.

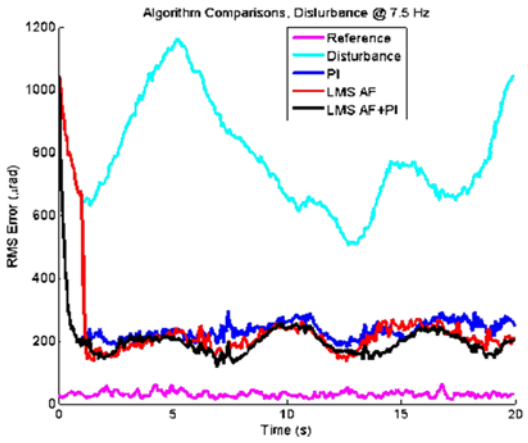


Fig. 16. Comparison of PI and LMS algorithms.

Table 1. Average RMS error for PI, LMS AF, LMS AF + PI.

Algoritm	Avg RMS Error (μrad)
LMS AF +PI	189.3
LMS AF	214.0
PI	238.8

RMS Error Results Using Modal Control

Modal control experiments are also performed with the testbed. Fig. 17 shows the RMS of the wavefront sensor error when the modal control method using **F** and **G** shown in Fig. 11 was applied. A PI controller is used for static aberrations and all 37 modes are controlled except for the orthogonal Zernike derivative and Zernike derivative bases where tip and tilt modes are excluded. Fig. 17 shows the resulting beam shape and the RMS error when the applied static aberration is corrected. The errors resulting from all bases functions used converge to the same value which is the minimum error that can be achieved with the given physical system.

Fig. 18 shows the effect of modal reduction when classical PI controller is used as a base controller. A dynamic disturbance was added into the AO system. The time mean of the RMS wavefront error is plotted against the number of modes used. When an appropriate modal basis is used, good AO performance can be achieved even with the reduced number of modes, which is directly related to the reduced number of control channels and computation required.

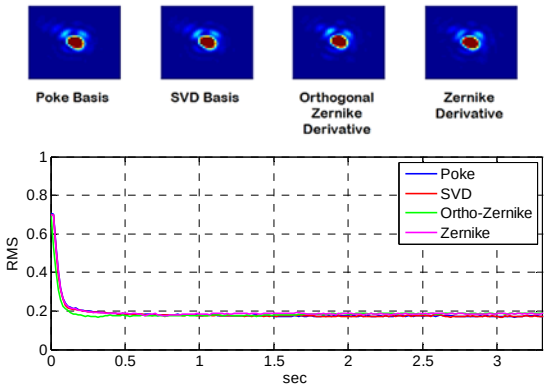


Fig. 17. RMS of the Error Vector Components When the Filtering of the Error Is Applied.

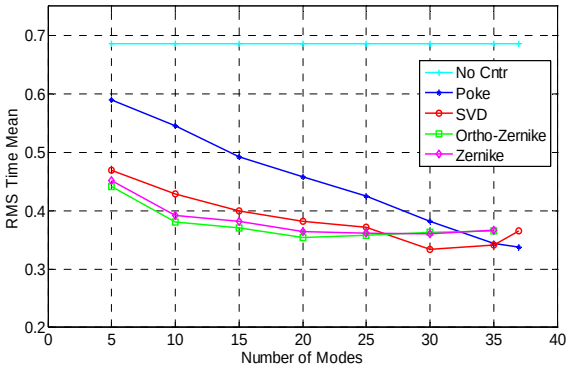


Fig. 18. Time mean of the sensor space error RMS by PI controller.

Fig. 19 shows the effectiveness of applying adaptive filter control in addition to the classical PI control and modal control. A similar dynamic disturbance was added into the AO system and the time mean of the RMS wavefront error plotted against the number of modes used. Compared to Fig. 18, time mean of the RMS wavefront error is lower with the addition of the adaptive filter control, which is effective in addressing dynamic disturbances. Similarly, good AO performance can be achieved with the reduced number of modes as well.

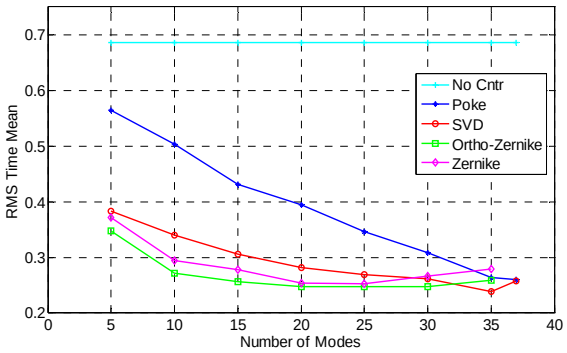


Fig. 19. Time mean of the sensor space error RMS by PI and RLS adaptive filter controller.

6. Conclusion

Meeting performance for optical beam jitter and wave front aberration is a very challenging problem. With the use of advanced sensors, actuators, and modern control techniques such as modal control and adaptive filter control techniques, the performance of optical beams can be significantly improved.

References

[1]. S. M. Kuo, D. R. Morgan, Active Noise Control Systems: Algorithms and DSP Implementations, *John Wiley & Sons, Inc.*, New York, 1996.

[2]. J. R. Watkins, B. N. Agrawal, Use of Least Mean Squares Filter in Control of Optical Beam Jitter, *AIAA Journal of Guidance, Control, and Dynamics*, Vol. 30, Issue 4, 2007, pp. 1116-1122.

[3]. http://cfao.ucolick.org/ao/how.php, accessed, March 29, 2018.

[4]. Elliott S. J., *et al*., A multiple error LMS Algorithm and its Application to the Active Control of Sound and Vibration, *IEEE Transactions on Acoustics, Speech, and Signal Processing*, Vol. 35, Issue 10, 1987, pp. 1423-1434.

[5]. M. Nagashima, J. Kim, B. Agrawal, Comparison of the Performance of Modal Control Schemes for an Adaptive Optics System and Analysis of the Effects of Actuator Limitations, in *Proceedings of the DEPS Beam Control Conference*, Broomfield, CO, 2012.

[6]. M. Nagashima, B. N. Agrawal, Application of Complex-valued FXLMS Adaptive Filter to Fourier Basis Control of Adaptive Optics, in *Proceedings of the American Control Conference*, San Francisco, CA, USA, Jun 2011, pp. 2939-2944.

[7]. M. S. Corley, M. Nagashima, B. N. Agrawal, Beam control and a New Laboratory Testbed for Adaptive Optics in a Maritime Environment, in *Proceedings of the IEEE Aerospace Conference*, Big Sky, MT, 2010.

[8]. B. Agrawal, J. J. Kim, Optical Beam Control for Jitter and Wavefront Aberrations, in *Proceedings of the 1st International Conference on Optics, Photonics and Laser (OPAL'2018)*, 9-11 May 2018, Barcelona, Spain, pp.33-39.

Published by International Frequency Sensor Association (IFSA) Publishing, S. L., 2018 (http://www.sensorsportal.com).